A Feedback Network Based High Step-Up Dc–Dc Converter for AC Photovoltaic Module Application

S.Lala Eswara Reddy[1], A.V.Suresh[2], O.V.S.Srinivasa Prasad[3]
M.Tech. Scholar[1], Assistant Professor[2], Professor[3]
Dept. of E.E.E., QIS Institute of Technology, Ongole, A.P., India.

***Abstract*—within the photovoltaic (PV) power-generation market, the ac PV module has shown obvious growth. However, a high voltage gain converter is essential for the module's grid connection through a dc–ac inverter. This paper proposes a converter that employs a floating active switch to isolate energy from the PV panel when the ac module is OFF; this particular design protects installers and users from electrical hazards. Without extreme duty ratios and the numerous turns-ratios of a coupled inductor, this converter achieves a high step-up voltage-conversion ratio; the leakage inductor energy of the coupled inductor is efficiently recycled to the load. These features explain the module's high-efficiency performance. The detailed operating principles and steady-state analyses of continuous, discontinuous, and boundary conduction modes are described. A 15 V input voltage, 230 V output voltage, prototype circuit of the proposed converter has been implemented; its maximum efficiency is up to 95.3% and full-load efficiency is 92.3%.**

***Index Terms*—AC module, coupled inductor, high step-up voltage gain, single switch.**

I. INTRODUCTION

PHOTOVOLTAIC (PV) power-generation systems are becoming increasingly important and prevalent in distribution generation systems. A conventional centralized PV array is a serial connection of numerous panels to obtain higher dc-link voltage for main electricity through a dc–ac inverter [1], [30]. Unfortunately, once there is a partial shadow on some panels, the system's energy yield becomes significantly reduced [2]. An ac module is a micro inverter configured on the rear bezel of a PV panel [1]–[3]; this alternative solution not only immunizes against the yield loss by shadow effect, but also provides flexible installation options in accordance with the user's budget [4]. Many prior research works have proposed a single-stage dc– ac inverter with fewer components to fit the dimensions of the bezel of the ac module, but their efficiency levels are lower than those of conventional PV inverters. The power capacity range of a single PV panel is about 100 W to 300 W, and the maxi-mum power point (MPP) voltage range is from 15 V to 40 V, which will be the input voltage of the ac module; in cases with lower input voltage, it is difficult for the ac module to reach high efficiency [3]. However, employing a high step-up dc–dc converter in the front of the inverter improves power-conversion efficiency and provides a stable dc link to the inverter.

When installing the PV generation system during daylight, for safety reasons, the ac module outputs zero voltage [4], [5]. Fig. 1 shows the solar energy through the PV panel and micro inverter to the output terminal when the switches are OFF. When installation of the ac module is taking place, this potential difference could pose hazards to both the worker and the facilities. A floating active switch is designed to isolate the dc current from the PV panel, for when the ac module is off-grid as well as in the non-operating condition. This isolation ensures the operation of the internal components without any residential energy being transferred to the output or input terminals, which could be unsafe.

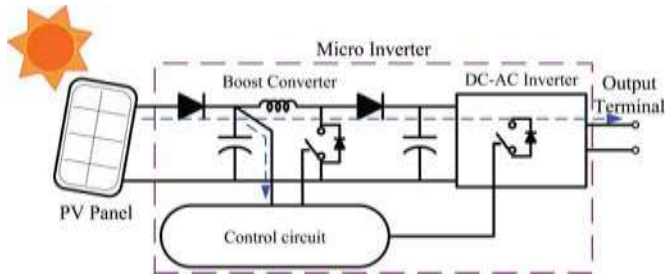

Fig. 1. Potential difference on the output terminal of nonfloating switch microinverter.

The micro inverter includes dc–dc boost converter, dc–ac inverter with control circuit as shown in Fig. 1. The dc–dc converter requires large step-up conversion from the panel's low voltage to the voltage level of the application. Previous research on various converters for high step-up applications has included analyses of the switched-inductor and switched-capacitor types [6], [7]; transformerless switched-capacitor type [8], [9], [29]; the voltage-lift type [12]; the capacitor-diode voltage multi-plier [13]; and the boost type integrated with a coupled inductor [10], [11], these converters by increasing turns ratio of coupled inductor obtain higher voltage gain than conventional boost converter. Some converters successfully combined boost and flyback converters, since various converter combinations are developed to carry out high step-up voltage gain by using the coupled-inductor technique [14]–[19], [27], [28]. The efficiency and voltage gain of the dc–dc boost converter are constrained by either the parasitic effect of the power switches or the reverse-recovery issue of the diodes. In addition, the

equivalent series resistance (ESR) of the capacitor and the parasitic resistances of the inductor also affect overall efficiency. Use of active clamp technique not only recycles the leakage inductor's energy but also constrains the voltage stress across the active switch; how-ever the tradeoff is higher cost and complex control circuit [25], [26]. By combining active snubber, auxiliary resonant circuit, synchronous rectifiers, or switched- capacitor-based resonant circuits and so on, these techniques made active switch into zero voltage switching (ZVS) or zero current switching (ZCS) operation and improved converter efficiency [20]–[24]. However, when the leakage-inductor energy from the coupled inductor can be recycled, the voltage stress on the active switch is reduced, which means the coupled inductor employed in combination with the voltage-multiplier or voltage-lift technique success-fully accomplishes the goal of higher voltage gain [6]–[13].

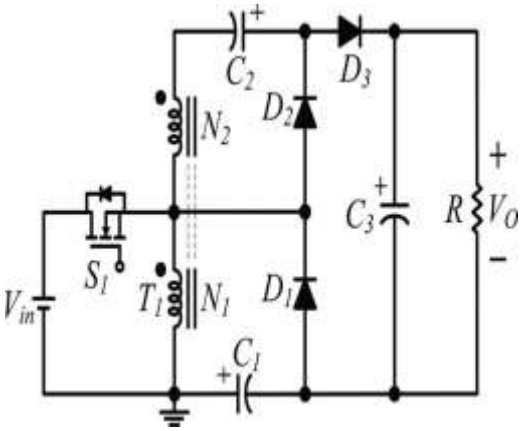

Fig. 2. Circuit configuration of proposed converter.

The proposed converter, shown in Fig. 2, is comprised of a coupled inductor T_1 with the floating active switch S_1. The primary winding N_1 of a coupled inductor T_1 is similar to the input inductor of the conventional boost converter, and capacitor C_1 and diode D_1 receive leakage inductor energy from N_1. The secondary winding N_2 of coupled inductor T_1 is connected with another pair of capacitors C_2 and diode D_2, which are in series with N_1 in order to further enlarge the boost voltage. The rectifier diode D_3 connects to its output capacitor C_3. The proposed converter has several features: 1) The connection of the two pairs of inductors, capacitor, and diode gives a large step-up voltage-conversion ratio; 2) the leakage-inductor energy of the coupled inductor can be recycled, thus increasing the efficiency and restraining the voltage stress across the active switch; and 3) the floating active switch efficiently isolates the PV panel energy during nonoperating conditions, which enhances safety. The operating principles and steady-state analysis of the proposed converter are presented in the following sections.

II. OPERATING PRINCIPLES OF THE PROPOSED CONVERTER

The simplified circuit model of the proposed converter is shown in Fig. 3. The coupled inductor T_1 is represented as a magnetizing inductor L_m, primary and secondary leakage inductors $L_{k\,1}$ and $L_{k\,2}$, and an ideal transformer. In order to simplify the circuit analysis of the proposed converter, the following assumptions are made.

1) All components are ideal, except for the leakage inductance of coupled inductor T_1, which is being taken under consideration. The on-state resistance $R_{D\,S\,(O\,N\,)}$ and all parasitic capacitances of the main switch S_1 are neglected, as are the forward voltage drops of diodes $D_1 \sim D_3$.
2) The capacitors $C_1 \sim C_3$ are sufficiently large that the voltages across them are considered to be constant.
3) The ESR of capacitors $C_1 \sim C_3$ and the parasitic resistance of coupled inductor T_1 are neglected.
4) The turns ratio n of the coupled inductor T_1 windings is equal to N_2 / N_1.

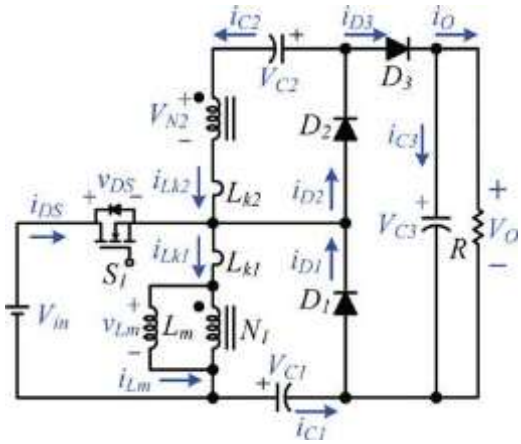

Fig. 3. Polarity definitions of voltage and current in proposed converter.

The operating principle of continuous conduction mode (CCM) is presented in detail. The current waveforms of major components are given in Fig. 4. There are five operating modes in a switching period. The operating modes are described as follows.

A. CCM Operation

Mode I [t_0, t_1]: In this transition interval, the magnetizing inductor L_m continuously charges capacitor C_2 through T_1 when S_1 is turned ON. The current flow path is shown in Fig. 5(a); switch S_1 and diode D_2 are conducting. The current $i_{L\,m}$ is de-creasing because source voltage V_{in} crosses magnetizing inductor L_m and primary leakage inductor $L_{k\,1}$; magnetizing inductor L_m is still transferring its energy through coupled

inductor T_1 to charge switched capacitor C_2, but the energy is decreasing; the charging current i_{D2} and i_{C2} are decreasing. The secondary leakage inductor current $i_{LK\ 2}$ is declining as equal to $i_{L\ m} / n$. Once the increasing $i_{L\ k\ 1}$ equals decreasing $i_{L\ m}$ at $t = t_1$, this mode ends.

Mode II [t_1, t_2]: During this interval, source energy V_{in} is series connected with N_2, C_1, and C_2 to charge output capacitor C_3 and load R; meanwhile magnetizing inductor L_m is also receiving energy from V_{in}. The current flow path is shown in Fig. 5(b), where switch S_1 remains ON, and only diode D_3 is conducting. The $i_{L\ m}$, $i_{L\ k\ 1}$, and $i_{D\ 3}$ are increasing because the V_{in} is crossing $L_{k\ 1}$, L_m , and primary winding N_1 ; L_m and $L_{k\ 1}$ are storing energy from V_{in} ; meanwhile V_{in} is also serially connected with secondary winding N_2 of coupled inductor T_1, capacitors C_1, and C_2, and then discharges their energy to capacitor C_3 and load R. The i_{in}, $i_{D\ 3}$ and discharging current $|i_{C\ 1}|$ and $|i_{C\ 2}|$ are increasing. This mode ends when switch S_1 is turned OFF at $t = t_2$.

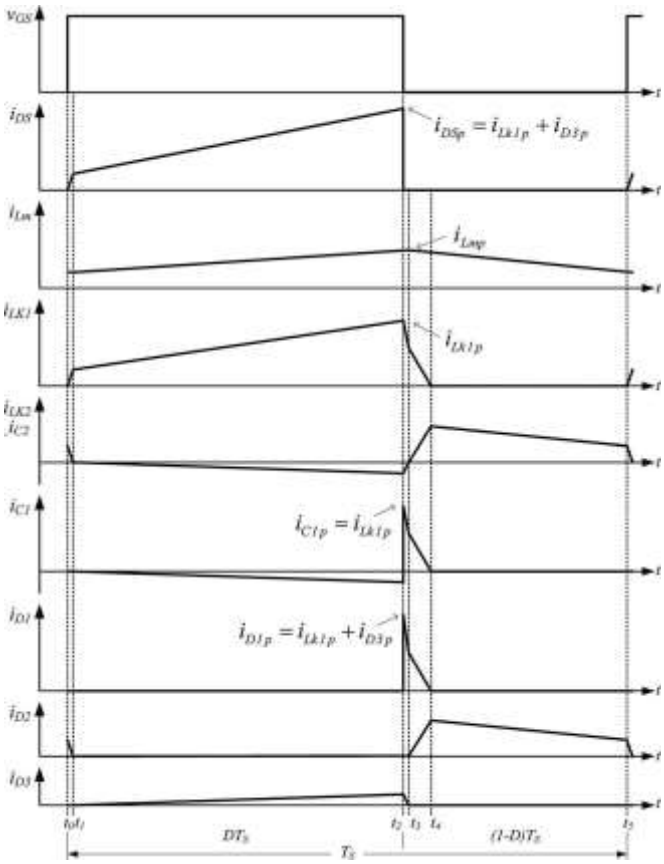

Fig. 4. Some typical waveforms of proposed converters at CCM operation.

Mode III [t_2, t_3]: During this transition interval, secondary leakage inductor $L_{k\ 2}$ keeps charging C_3 when switch S_1 is OFF. The current flow path is shown in Fig. 5(c), where only diode D_1 and D_3 are conducting. The energy stored in leakage inductor L_{k1} flows through diode D_1 to charge capacitor C_1 instantly when S_1 is OFF. Meanwhile, the energy of secondary leakage inductor $L_{k\ 2}$ is series connected with C_2 to charge output capacitor C_3 and the load. Because leakage inductance $L_{k\ 1}$ and $L_{K\ 2}$ are far smaller than L_m, $i_{L\ k\ 2}$ rapidly decreases, but $i_{L\ m}$ is increasing because magnetizing inductor L_m is receiving energy from $L_{k\ 1}$. Current $i_{L\ k\ 2}$ decreases until it reaches zero; this mode ends at $t = t_3$.

Mode IV [t_3, t_4]: During this transition interval, the energy stored in magnetizing inductor L_m is released to C_1 and C_2 simultaneously. The current flow path is shown in Fig. 5(d). Only diodes D_1 and D_2 are conducting. Currents $i_{L\ k\ 1}$ and $i_{D\ 1}$ are continually decreased because the leakage energy still flowing through diode D_1 keeps charging capacitor C_1. The L_m is delivering its energy through $T_{\ 1}$ and D_2 to charge capacitor C_2. The energy stored in capacitor C_3 is constantly discharged to the load R. These energy transfers result in decreases in $i_{L\ k\ 1}$ and $i_{L\ m}$ but increases in $i_{L}\ k_2$. This mode ends when current i_{Lk1} is zero, at $t = t_4$.

Mode V [t_4, t_5]: During this interval, only magnetizing inductor L_m is constantly releasing its energy to C_2. The current flow path is shown in Fig. 5(e), in which only diode D_2 is con-ducting. The $i_{L\ m}$ is decreasing due to the magnetizing inductor energy flowing through the coupled inductor T_1 to secondary winding N_2, and D_2 continues to charge capacitor C_2. The energy stored in capacitor C_3 is constantly discharged to the load R. This mode ends when switch S_1 is turned ON at the beginning of the next switching period.

B. DCM Operation

The detailed operating principles for discontinuous-conduction-mode (DCM) operation are presented in this section. Fig. 6 depicts several typical waveforms during five operating modes of one switching period. The operating modes are de-scribed as follows.

Mode I [t_0, t_1]: During this interval, source energy V_{in} is series connected with N_2, C_1, and C_2 to charge output capacitor C_3 and load R; meanwhile, magnetizing inductor L_m is also receiving energy from V_{in}. The current flow path is shown in Fig. 7(a), which depicts that switch S_1 remains ON, and only diode D_3 is conducting. The $i_{L\ m}$, $i_{L\ k\ 1}$, and $i_{D\ 3}$ are increasing because the V_{in} is crossing $L_{k\ 1}$, L_m, and primary winding N_1; L_m and $L_{k\ 1}$ are storing energy from V_{in}; meanwhile, V_{in} also is serially connected with secondary winding N_2 of coupled inductor T_1, capacitors C_1, and C_2; then they all discharge their energy to capacitor C_3 and load R. The i_{in} , $i_{D\ 3}$ and

discharging current $|i_{C\,1}|$ and $|i_{C\,2}|$ are increasing. This mode ends when switch S_1 is turned OFF at $t = t_1$.

Mode II [t_1, t_2]: During this transition interval, secondary leakage inductor $L_{k\,2}$ keeps charging C_3 when switch S_1 is OFF. The current flow path is shown in Fig. 7(b), and only diode D_2 and D_3 are conducting. The energy stored in leakage inductor

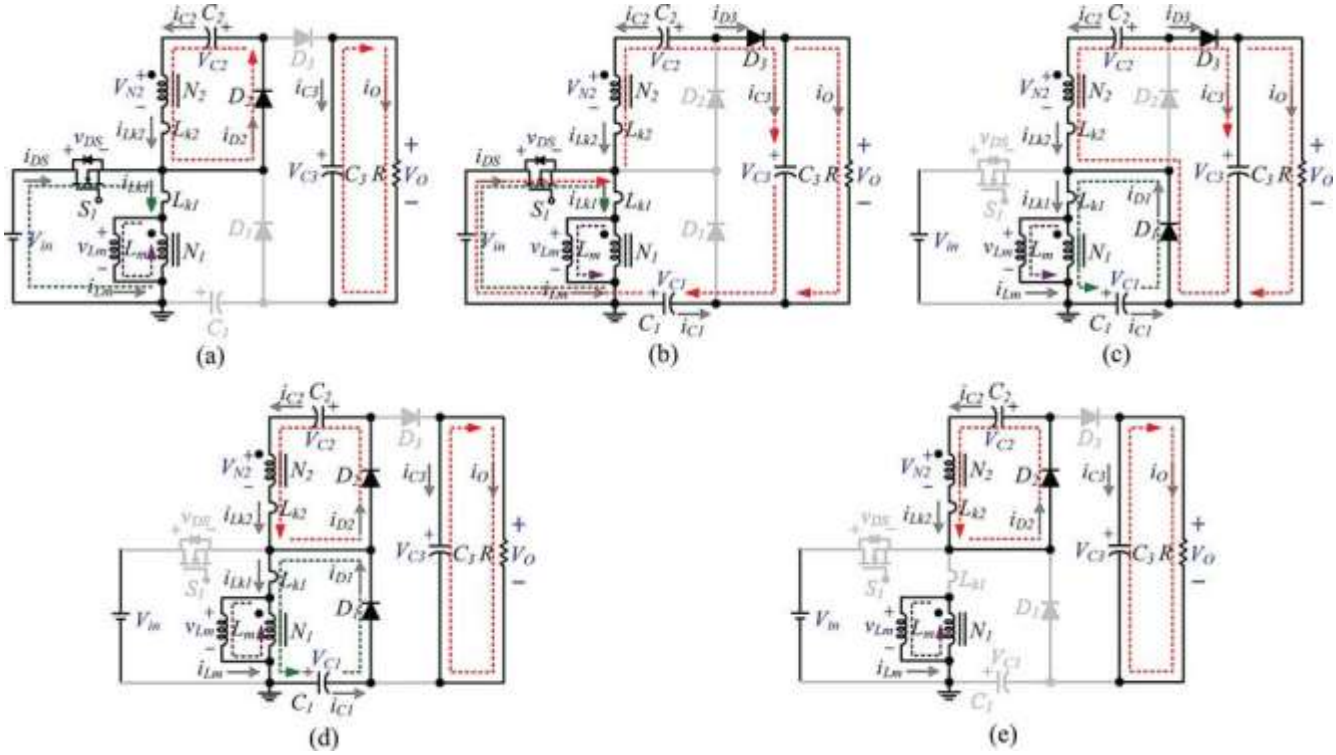

Fig. 5. Current flow path of five operating modes during one switching period at CCM operation. (a) Mode I: $t_0 \sim t_1$. (b) Mode II: $t_1 \sim t_2$. (c) Mode III: $t_2 \sim t_3$. (d) Mode IV: $t_3 \sim t_4$. (e) Mode V: $t_4 \sim t_5$.

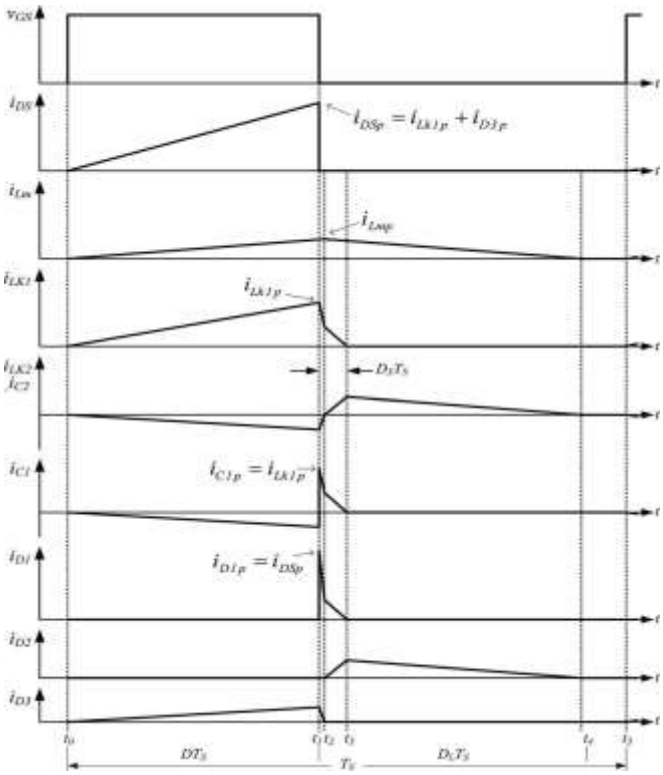

Fig. 6. Some typical waveforms of proposed converters at DCM operation

$L_{k\,1}$ flows through diode D_1 to charge capacitor C_1 instantly when S_1 is OFF. Meanwhile, the energy of secondary leakage inductor $L_{k\,2}$ is series-connected with C_2 to charge output capacitor C_3 and the load. Because leakage inductance $L_{k\,1}$ and $L_{K\,2}$ are far smaller than L_m, $i_{Lk\,2}$ decreases rapidly, but $i_{L\,m}$ is increasing because magnetizing inductor L_m is receiving energy from $L_{k\,1}$ Current $i_{L\,k\,2}$ reduces down to zero, and this mode ends at $t = t_2$.

Mode III [t2, t3]: During this transition interval, the energy stored in coupled inductor T_1 is releasing to C_1 and C_2. The current flow path is shown in Fig. 7(c). Only diodes D_1 and D_2 are conducting. Currents i_{lk1} and i_{D1} are continually decreased because leakage energy still flowing through diode D_1 keeps charging capacitor C_1. The L_m is delivering its energy through T_1 andD_2 to charge capacitorC_2 .The energy stored in capacitor C_3 is constantly discharged to the load R. These energy transfers result in decreases in i_{LK1} and i_{Lm} but increases in i_{Lk2}. This mode ends when current i_{Lk1} reaches zero at $t = t_3$.

Mode IV [t_3, t_4]: During this interval, only magnetizing inductor L_m is constantly releasing its energy to C_2. The current flow path is shown in Fig.7(d), and only diode D_2 is conducting. The i_{lm} s decreasing due to the magnetizing inductor energy flowing through the coupled inductor T_1 to secondary winding N_2, and D_2 continues to charge capacitor C_2. The energy stored in capacitor C_3 is constantly discharged to the load R. This mode ends when current $i_{L\,m}$ reaches zero at t=t_4.

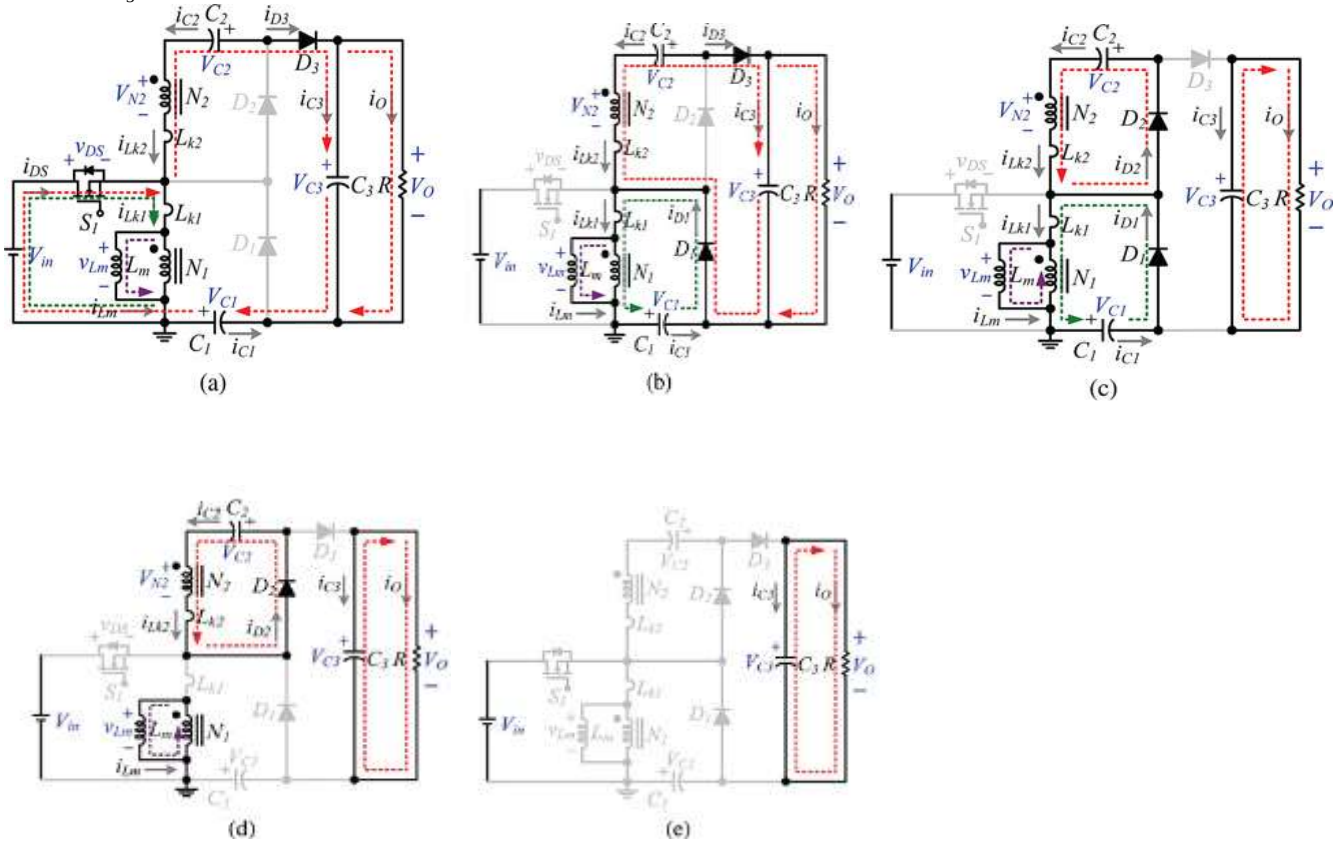

Fig. 7. Current flow path of five operating modes during one switching period at DCM operation. (a) Mode I: $t_0 \sim t_1$. (b) Mode II: $t_1 \sim t_2$. (c) Mode III: $t_2 \sim t_3$. (d) Mode IV: $t_3 \sim t_4$. (e) Mode V: $t_4 \sim t_5$.

Mode V [t_4, t_5]: During this interval, all active components are turned OFF; only the energy stored in capacitor C_3 is continued to be discharged to the load R. The current flow path is shown in Fig. 7(e). This mode ends when switch S_1 is turned ON at the beginning of the next switching period

III. STEADY-STATE ANALYSIS OF PROPOSED CONVERTERS

To simplify the steady-state analysis, only modes II and IV are considered for CCM operation, and the leakage inductances on the secondary and primary sides are neglected. The following equations can be written from fig 5(b):

$$v_{\mathrm{Lm}} = V_{\mathrm{in}} \qquad (1)$$

$$v_{\mathrm{N2}} = nV_{\mathrm{in}} \qquad (2)$$

During mode IV, $v_{\mathrm{Lm}} = -V_{\mathrm{c1}}$ (3)

$$v_{\mathrm{N2}} = -V_{\mathrm{c2}} \qquad (4)$$

Applying a volt-second balance on the magnetizing inductor L_m yields

$$\int_0^{DT_s}(V_{in})dt + \int_{DT_s}^{T_s}(-V_{C1})dt = 0 \quad (5)$$

$$\int_0^{DT_s}(nV_{in})dt + \int_{DT_s}^{T_s}(-v_{C2})dt = 0 \quad (6)$$

From which the voltage across capacitors *C*1 and *C*2 are obtained as follows:

$$V_{c1} = \frac{D}{1-D}V_{in} \quad (7)$$

$$V_{c2} = \frac{nD}{1-D}V_{in} \quad (8)$$

During mode II, the output voltage $V_O = V_{in} + V_{N2} + V_{C2} + V_{C1}$ becomes

$$V_0 = V_{in} + nV_{in} + \frac{nD}{1-D}V_{in} + \frac{D}{1-D}V_{in} \quad (9)$$

The DC voltage gain M_{CCM} can be found as follows:

$$M_{CCM} = \frac{V_0}{V_{in}} = \frac{1+n}{1-D} \quad (10)$$

Both [10] and [11] are employing coupled inductor topology as the boost type converter integrating with coupled inductor; this technology is similar to the technology of the proposed converter. Fig.8 shows the plot of voltage gain M_{CCM} as function of duty ratio *D* of the proposed converter is compared with that of available converters [10],[11]. The chart reveals the voltage gain CCM of proposed converter is obviously higher than available converters. All of them are operating under the same conditions: CCM and *n* = 5.During CCM operation, the voltage stresses on S1 and *D*1~*D*3 are given as

$$V_{DS} = V_{D1} = \frac{V_{in}}{1-D} \quad (11)$$

$$V_{D2} = \frac{nV_{in}}{1-D} \quad (12)$$

$$V_{D3} = \frac{1+n}{1-D}V_{in} \quad (13)$$

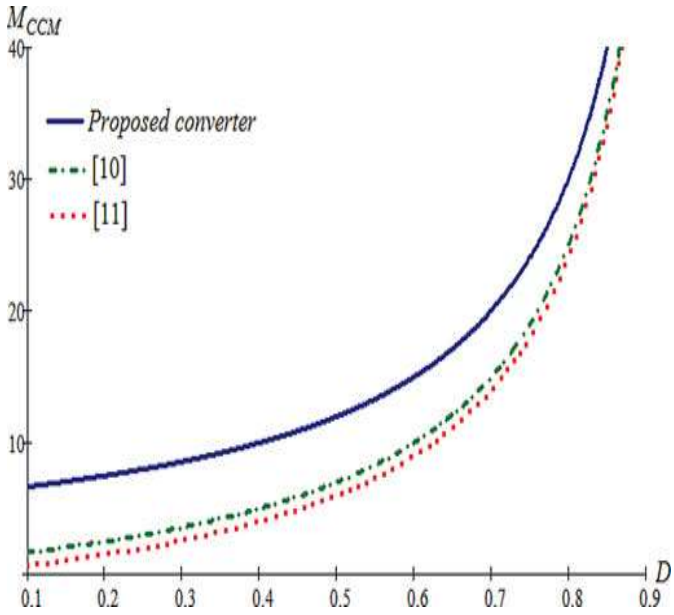

Fig. 8. Voltage gain as a function of the duty ratio of the proposed converter. [10] and [11] under CCM operation and *n* = 5.

IV. EXPERIMENTAL RESULTS

A 100Wprototype sample is presented to verify the practicability of the proposed converter. The electrical specifications are *V*in = 15V, *VO* = 230V, *fS* = 50 kHz, and full-load resistance *R* = 400 Ω. The major components required are *C*1 = *C*2 =47 μF and *C*3 = 550 μF. The main switch *S*1 is a MOSFETIXFK180N15P, the diodes *D*1 are MRB20200CTG, and the DPG30C300HB is selected for *D*2 and *D*3. Since (10) assign turns ratio *n* = 5, the duty ratio *D* is derived as 55%.

The boundary normalized magnetizing inductor time constant τLB is found by (28) to be 1.547 ×10−3. To define the proposed converter's BCM operation at 50% of the full load, the load resistance *R* = 400 Ω.

The actual inductance of magnetizing inductor L_m of the coupled inductor is 30.54 μH, which is larger than boundary magnetizing inductance 24.75 μH. Fig. 11 shows voltage and current waveforms, which are measured from active switch S_1 , diodes D_1 , D_2 , and D_3 , and the current waveforms of C_1 and C_2 . The measured voltage spike across the active switch is found to be about 80 V; this reveals that the energy of the leakage inductor has been stored in and voltage clamped by C_1. These experimental waveforms agree with the operating principles and the steady-state analysis. Fig. 12 shows that the maximum efficiency of 95.3% occurred at 40% of full load; and the full-load efficiency is maintained at 92.3%. The

efficiency variation is about 3%, and the flat efficiency curve is able to yield higher energy from the PV module during periods when sunlight is fading. The residential voltage discharge time of the proposed converter is 480 milliseconds, which prevents any potential electrical injuries to humans.

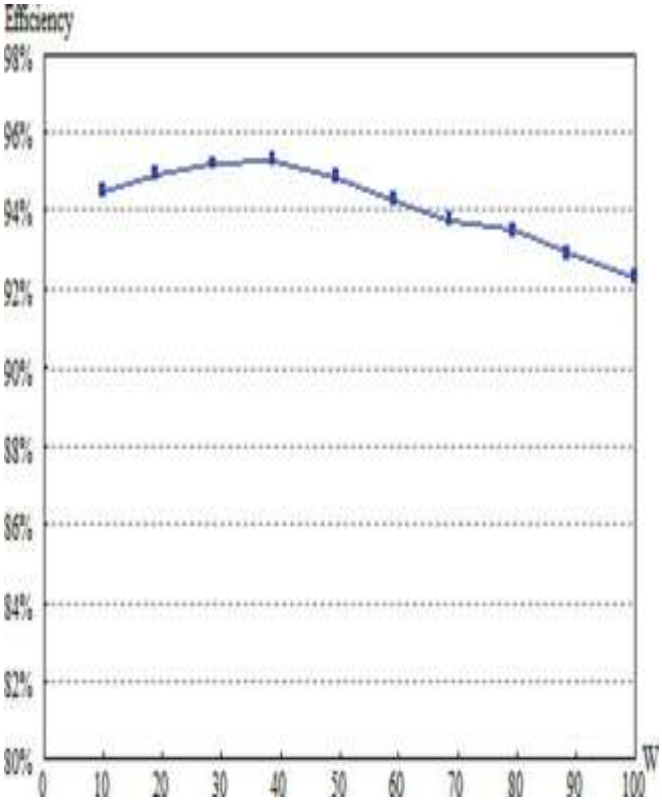

Fig. 9. Measured efficiency of proposed converter

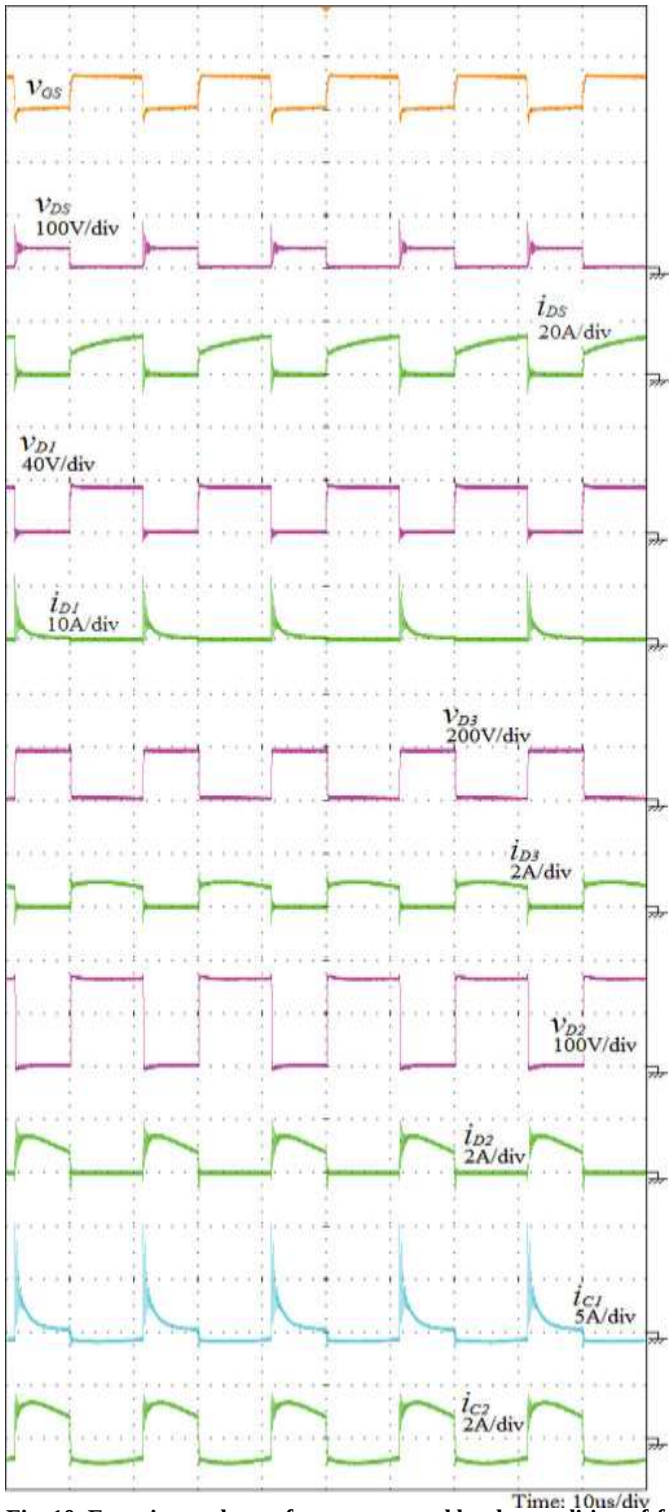

Fig. 10. Experimental waveforms measured by the condition of f_S = 50 kHz, V_{in} = 15 V,

V. IMPLEMENTATION OF FEEDBACK NETWORK OF PROPOSED CONVERTER

A feedback network based high step-up dc-dc converter is shown in Fig.12 which is used to increase the output voltage as compared to high step up dc-dc converter. It consists of gain, integrator, saturation, relational operator, adder and logical operator. The closed loop circuit which sense the output voltage of high step-up dc-dc converter and compare with input voltage. The output voltage is feedback and compare with a constant of 230. The will give error voltage which compare the both the voltages. The Gain block multiplies the input by a constant value. The Integrator block outputs the value of the integral of its input signal with respect to time. The Saturation block imposes upper and lower limits on an input signal. The Repeating Sequence block outputs a periodic scalar signal having a waveform that you specify using the time values and output values parameters. The relational operator set True if first input less than or equal to second input. The output equals 1 for TRUE and 0 for FALSE. The output of Relational operator is true the output of NOT operator is False and vice versa. The output logical operator is connected to gate of mosfet. The switch will modify the output voltage of high step-up DC-DC converter as per our requirement.

Simulation result:

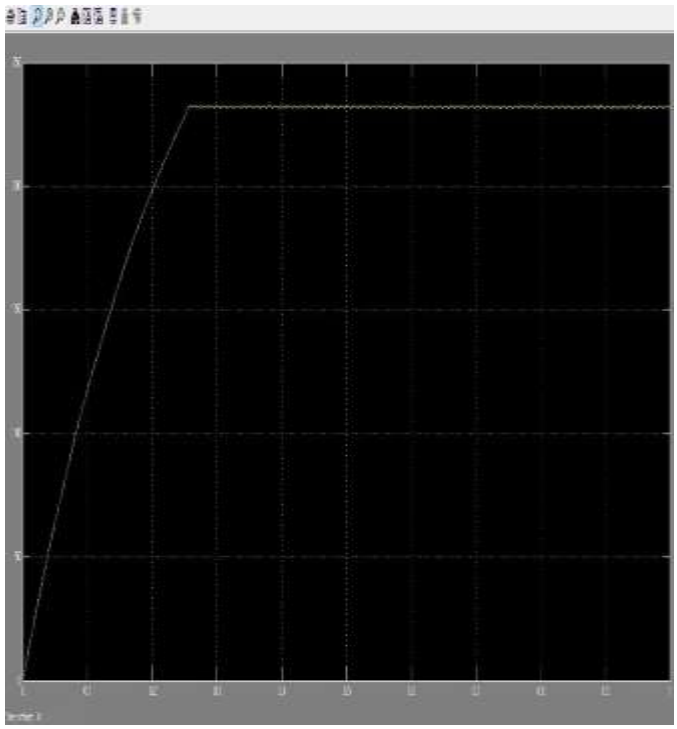

Fig.11 output voltage waveform

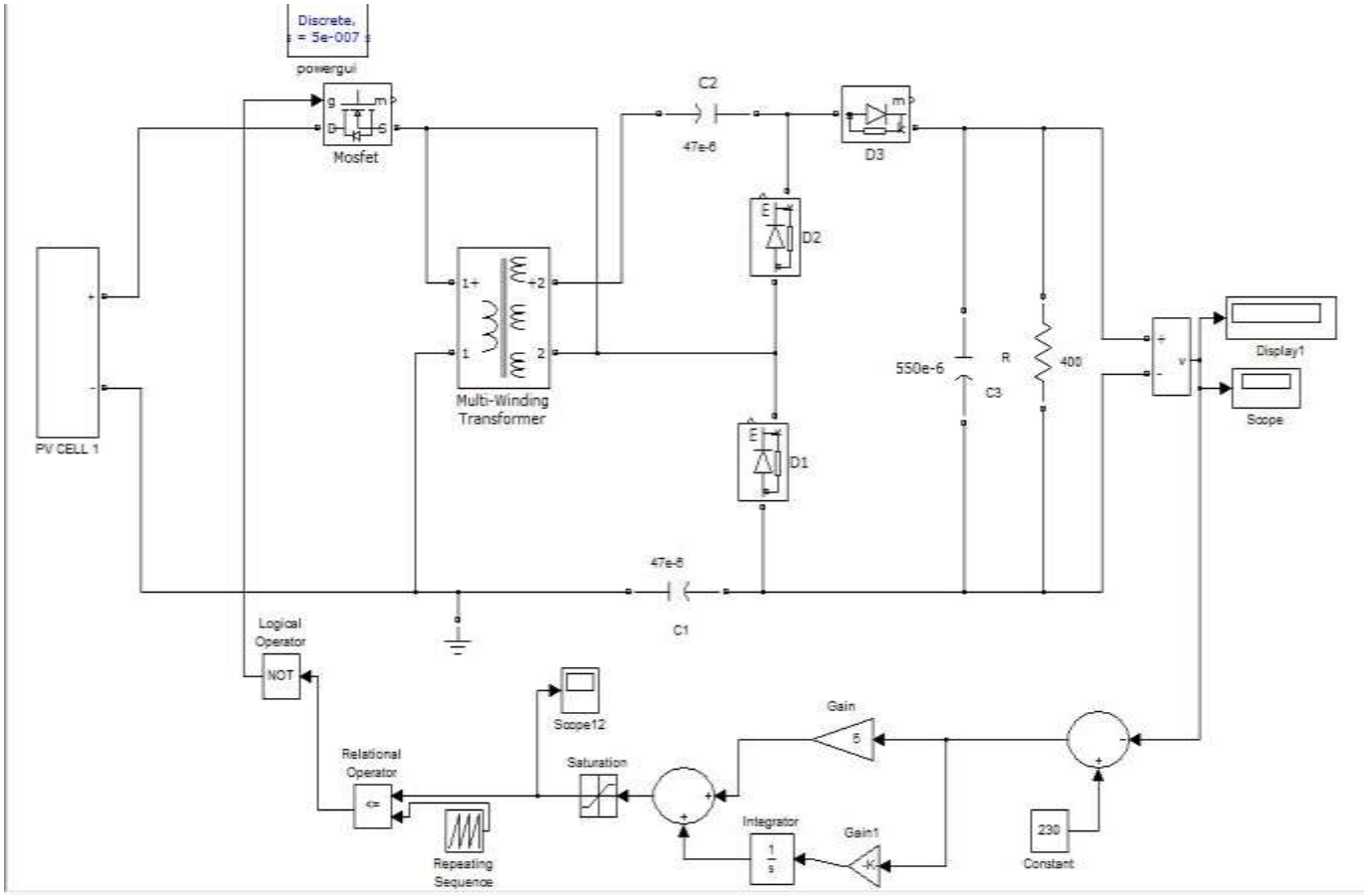

Fig12.feedback network of proposed converter

VI. CONCLUSION

Since the energy of the coupled inductor's leakage inductor has been recycled, the voltage stress across the active switch S_1 is constrained, which means low ON-state resistance $R_{DS(ON)}$ can be selected. Thus, improvements to the efficiency of the proposed converter have been achieved. The switching signal action is performed well by the floating switch during system operation; on the other hand, the residential energy is effectively eliminated during the nonoperating condition, which improves safety to system. From the prototype converter, the turns ratio n = 5 and the duty ratio D is 55%; thus, without extreme duty ratios and turns ratios, the proposed converter achieves high step-up voltage gain, of up to 13 times the level of input voltage. The experimental results show that the maximum efficiency of 95.3% is measured at half load, and a small efficiency variation will harvest more energy from the PV module during fading sunlight.

REFERENCES

[1] T. Shimizu, K. Wada, and N. Nakamura, "Flyback-type single-phase utility interactive inverter with power pulsation decoupling on the dc input for an ac photovoltaic module system," *IEEE Trans. Power Electron.*, vol. 21, no. 5, pp. 1264–1272, Jan. 2006.

[2] C. Rodriguez and G. A. J. Amaratunga, "Long-lifetime power inverter for photovoltaic ac modules," *IEEE Trans. Ind. Electron.*, vol. 55, no. 7, pp. 2593–2601, Jul. 2008.

[3] S. B. Kjaer, J. K. Pedersen, and F. Blaabjerg, "A review of single-phase grid-connected inverters for photovoltaic modules," *IEEE Trans. Ind. Appl.*, vol. 41, no. 5, pp. 1292–1306, Sep./Oct. 2005.

[4] J. J. Bzura, "The ac module: An overview and update on self-contained modular PV systems," in *Proc. IEEE Power Eng. Soc. Gen. Meeting*, Jul. 2010, pp. 1–3.

[5] B. Jablonska, A. L. Kooijman-van Dijk, H. F. Kaan, M. van Leeuwen, G.

T. M. de Boer, and H. H. C. de Moor, "PV-PRIVE project at ECN, five years of experience with small-scale ac module PV

systems," in *Proc. 20th Eur. Photovoltaic Solar Energy Conf.*, Barcelona, Spain, Jun. 2005, pp. 2728–2731.

[6] T. Umeno, K. Takahashi, F. Ueno, T. Inoue, and I. Oota, "A new approach to low ripple-noise switching converters on the basis of switched- capacitor converters," in *Proc. IEEE Int. Symp. Circuits Syst.*, Jun. 1991, pp. 1077– 1080. -2, pp. 687–696, Mar. 2008.

[7] B. Axelrod, Y. Berkovich, and A. Ioinovici, "Switched-capacitor/ switched-inductor structures for getting transformerless hybrid dc–dc PWM converters," *IEEE Trans. Circuits Syst. I, Reg. Papers*, vol. 55, no

[8] . B. Axelrod, Y. Berkovich, and A. Ioinovici, "Transformerless dc–dc con-verters with a very high dc line-to-load voltage ratio," in *Proc. IEEE Int. Symp. Circuits Syst. (ISCAS)*, 2003, vol. 3, pp. 435–438.

[9] H. Chung and Y. K. Mok, "Development of a switched-capacitor dc–dc boost converter with continuous input current waveform," *IEEE Trans. Circuits Syst. I, Fundam. Theory Appl.*, vol. 46, no. 6, pp. 756–759, Jun. 1999.

[10] T. J. Liang and K. C. Tseng, "Analysis of integrated boost-flyback step-up converter," *IEE Proc. Electrical Power Appl.*, vol. 152, no. 2, pp. 217–225, Mar. 2005.

[11] Q. Zhao and F. C. Lee, "High-efficiency, high step-up dc–dc converters," *IEEE Trans. Power Electron.*, vol. 18, no. 1, pp. 65–73, Jan. 2003.

[12] M. Zhu and F. L. Luo, "Voltage-lift-type cuk converters: Topology and analysis," *IET Power Electron.*, vol. 2, no. 2, pp. 178–191, Mar. 2009

[13] . J. W. Baek, M. H. Ryoo, T. J. Kim, D. W. Yoo, and J. S. Kim, "High boost converter using voltage multiplier," in *Proc. IEEE Ind. Electron. Soc. Conf. (IECON)*, 2005, pp. 567–572.

[14] J. Xu, "Modeling and analysis of switching dc–dc converter with coupled-inductor," in *Proc. IEEE 1991 Int. Conf. Circuits Syst. (CICCAS)*, 1991, 717–720.

[15] R. J. Wai, C. Y. Lin, R. Y. Duan, and Y. R. Chang, "High-efficiency dc–dc converter with high voltage gain and reduced switch stress," *IEEE Trans. Ind. Electron.*, vol. 54, no. 1, pp. 354–364, Feb. 2007.

[16] S. M. Chen, T. J. Liang, L. S. Yang, and J. F. Chen, "A cascaded high step-up dc–dc converter with single switch for microsource applications," *IEEE Trans. Power Electron.*, vol. 26, no. 4, pp. 1146–1153, Apr. 2011.

[17] T. J. Liang, S. M. Chen, L. S. Yang, J. F. Chen, and A. Ioinovici, "Ultra large gain step-up switched-capacitor dc–dc converter with coupled inductor for alternative sources of energy," *IEEE Trans. Circuits Syst. I*, to be published.

[18] L. S. Yang and T. J. Liang, "Analysis and implementation of a novel bidirectional dc–dc converter," *IEEE Trans. Ind. Electron.*, vol. 59, no. 1, 422–434, Jan. 2012.

[19] W. Li and X. He, "Review of non-isolated high-step-up dc/dc converters in photovoltaic grid-connected applications," *IEEE Trans. Ind. Electron.*, vol. 58, no. 4, pp. 1239–1250, Apr. 2011.

[20] S. H. Park, S. R. Park, J. S. Yu, Y. C. Jung, and C. Y. Won, "Analysis and design of a soft-switching boost converter with an HI-Bridge auxiliary resonant circuit," *IEEE Trans. Power Electron.*, vol. 25, no. 8, pp. 2142– 2149, Aug. 2010.

[21] G. Yao, A. Chen, and X. He, "Soft switching circuit for interleaved boost converters," *IEEE Trans. Power Electron.*, vol. 22, no. 1, pp. 80–86, Jan. 2007.

[22] Y. Park, S. Choi, W. Choi, and K. B. Lee, "Soft-switched interleaved boost converters for high step-up and high power applications," *IEEE Trans. Power Electron.*, vol. 26, no. 10, pp. 2906–2914, Oct. 2011.

[23] Y. Zhao, W. Li, Y. Deng, and X. He, "Analysis, design, and experimenta-tion of an isolated ZVT boost converter with coupled inductors," *IEEE Trans. Power Electron.*, vol. 26, no. 2, pp. 541–550, Feb. 2011.

[24] H. Mao, O. Abdel Rahman, and I. Batarseh, "Zero-voltage-switching dc– dc converters with synchronous rectifiers," *IEEE Trans. Power Electron.*, vol. 23, no. 1, pp. 369–378, Jan. 2008.

[25] J. M. Kwon and B. H. Kwon, "High step-up active-clamp converter with input-current doubler and output-voltage doubler for fuel cell power sys-tems," *IEEE Trans. Power Electron.*, vol. 24, no. 1, p. 108–115, Jan. 2009.

[26] S. Dwari and L. Parsa, "An efficient high-step-up interleaved dc–dc con-verter with a common active clamp," *IEEE Trans. Power Electron.*, vol. 26, no. 1, pp. 66–78, Jan. 2011.

[27] C. Restrepo, J. Calvente, A. Cid, A. El Aroudi, and R. Giral, "A non-inverting buck-boost dc–dc switching converter with high efficiency and wide bandwidth," *IEEE Trans. Power Electron.*, vol. 26, no. 9, pp. 2490– 2503, Sep. 2011.

[28] K. B. Park, G. W. Moon, and M. J. Youn, "Nonisolated high step-up boost converter integrated with sepic converter," *IEEE Trans. Power Electron.*, vol. 25, no. 9, pp. 2266–2275, Sep. 2010.

[29] L. S. Yang, T. J. Liang, and J. F. Chen, "Transformerless dc–dc converters with high step-up voltage gain," *IEEE Trans. Ind. Electron.*, vol. 56, no. 8, 3144–3152, Aug. 2009.

[30] N. Pogaku, M. Prodanovic, and T. C. Green, "Modeling, analysis and testing of autonomous operation of an inverter-based microgrid," *IEEE Trans. Power Electron.*, vol. 22, no. 2, pp. 613–625, Mar. 2007.

AUTHOR DETAILS

S.LALA ESWARA REDDY currently pursuing his M.Tech. in power electronics and drives in Qis institute of technology, Ongole, Andhra Pradesh, affiliated to JNTU, Kakinada. He has done his B.Tech. Degree from Krishna Chaitanya institute of technology and sciences, markapuram affiliated to JNTU, Kakinada, Andhra Pradesh, India and his fields of interest include renewable energy sources, power electronic drives.

A.V.SURESH presently working as Assistant Professor in Qis institute of technology, Ongole, Andhra Pradesh, India. He had completed his M.Tech. in Qis College of Engineering and Technology, Ongole, Andhra Pradesh. His fields of interest include advanced control systems and power systems.

O.V.S.SRINIVASA PRASAD currently working as Professor & H.O.D of electrical and electronics engineering department in Qis institute of technology, Ongole, Andhra Pradesh, India. He had completed his M.E. Gulbarga University, kalaburagi, Karnataka. His fields of interest include Power Electronics and Drives.

